

Parameterizing Scalar Transfer over Snow and Ice: A Review

EDGAR L ANDREAS

U.S. Army Cold Regions Research and Engineering Laboratory, Hanover, New Hampshire

(Manuscript received 12 October 2001, in final form 28 February 2002)

ABSTRACT

Evaluating the profiles of wind speed, temperature, and humidity in the atmospheric surface layer or modeling the turbulent surface fluxes of sensible and latent heat over horizontally homogeneous surfaces of snow or ice requires five pieces of information. These are the roughness lengths for wind speed (z_0), temperature (z_T), and humidity (z_Q) and the stratification corrections for the wind speed and scalar profiles ψ_m and ψ_h , respectively. Because over snow and ice the atmospheric surface layer is often stably stratified, the discussion here focuses first on which of the many suggested ψ_m and ψ_h functions to use over snow and ice. On the basis of four profile metrics—the critical Richardson number, the Deacon numbers for wind speed and temperature, and the turbulent Prandtl number—the manuscript recommends the Holtslag and de Bruin ψ_m and ψ_h functions because these have the best properties in very stable stratification. Next, a reanalysis of five previously published datasets confirms the validity of a parameterization for z_T/z_0 as a function of the roughness Reynolds number (R_*) that the author reported in 1987. The z_T/z_0 data analyzed here and that parameterization are compatible for R_* values between 10^{-4} and 100, which span the range from aerodynamically smooth through aerodynamically rough flow. Discussion of a z_0 parameterization is deferred and an insufficiency of data for evaluating z_Q is reported, although some z_Q data is presented.

1. Introduction

Over glaciers, sea ice, and snow-covered ground, the atmospheric surface layer is often stably stratified. Estimating the contributions from the surface sensible and latent heat fluxes to the surface energy budget for such surfaces usually relies on Monin–Obukhov similarity theory to deal with these stratification effects. This method, in turn, requires knowing how to parameterize the roughness lengths for wind speed (z_0), the so-called scalar roughness length for temperature (z_T) and humidity (z_Q), and the stratification corrections to the usual semilogarithmic profiles for wind speed, temperature, and humidity.

Mathematically, in the context of Monin–Obukhov similarity theory, the profiles for wind speed (U), potential temperature (T), and specific humidity (Q) as functions of height (z) in the atmospheric surface layer obey

$$U(z) = \frac{u_*}{k} \left[\ln \left(\frac{z}{z_0} \right) - \psi_m \left(\frac{z}{L} \right) \right], \quad (1.1a)$$

$$T(z) = T_s + \frac{t_*}{k} \left[\ln \left(\frac{z}{z_T} \right) - \psi_h \left(\frac{z}{L} \right) \right], \quad (1.1b)$$

$$Q(z) = Q_s + \frac{q_*}{k} \left[\ln \left(\frac{z}{z_Q} \right) - \psi_h \left(\frac{z}{L} \right) \right]. \quad (1.1c)$$

Here, k ($=0.40$) is the von Kármán constant; T_s and Q_s are the temperature and specific humidity at the surface; L is the Obukhov length, a stratification parameter; and ψ_m and ψ_h are the stratification corrections to the semi-logarithmic profiles. In (1.1c), I make the usual assumption that ψ_h is the same for both the temperature and humidity profiles. Over surfaces of snow and ice, we commonly take Q_s to be the saturation specific humidity at temperature T_s .

Last, in (1.1), u_* is the friction velocity, and t_* and q_* are analogous temperature and humidity flux scales such that the sensible (H_s) and latent (H_L) heat fluxes are

$$H_s = -\rho c_p u_* t_*, \quad (1.2a)$$

$$H_L = -\rho L_v u_* q_*. \quad (1.2b)$$

Here, ρ is the air density; c_p , the specific heat of air at constant pressure; and L_v , the latent heat of vaporization or sublimation. Since this review concentrates on stable stratification, I follow Nieuwstadt (1984) and treat u_* , t_* , q_* , and L as local scales.

Combining (1.1) and (1.2) results in the usual bulk-aerodynamic method for estimating H_s and H_L :

$$H_s = \rho c_p C_{H_z} U(z) [T_s - T(z)], \quad (1.3a)$$

$$H_L = \rho L_v C_{E_z} U(z) [Q_s - Q(z)]. \quad (1.3b)$$

Here, C_{H_z} and C_{E_z} are called the scalar transfer coefficients: the transfer coefficients for sensible and latent heat at reference height z . Combining (1.1), (1.2), and (1.3), we evaluate these coefficients to be

Corresponding author address: Dr. Edgar L Andreas, U.S. Army Cold Regions Research and Engineering Laboratory, 72 Lyme Road, Hanover, NH 03755-1290.
E-mail: eandreas@crrel.usace.army.mil

$$C_{H_z} = \frac{k^2}{[\ln(z/z_0) - \psi_m(\zeta)][\ln(z/z_T) - \psi_h(\zeta)]}, \quad (1.4a)$$

$$C_{E_z} = \frac{k^2}{[\ln(z/z_0) - \psi_m(\zeta)][\ln(z/z_Q) - \psi_h(\zeta)]}, \quad (1.4b)$$

where $\zeta = z/L$.

Thus, to reiterate, estimating H_s and H_L , in general, requires knowing how to parameterize the roughness lengths z_0 , z_T , and z_Q and the stratification corrections ψ_m and ψ_h . My focus here is on how to parameterize z_T and z_Q over surfaces of ice or snow. The subject of how to parameterize z_0 over such surfaces is much more complex and must await a dedicated review, although Kind (1976), Jackson and Carroll (1978), Banke et al. (1980), Chamberlain (1983), Inoue (1989), Raupach (1992), Andreas and Claffey (1995), and Andreas (1995), among many others, offer insights into this parameterization.

Finding z_T and z_Q involves either calculating C_{H_z} and C_{E_z} from measurements of H_s and H_L using (1.3) and then solving (1.4) for z_T and z_Q or fitting profile measurements with (1.1) to obtain the flux scales and the roughness lengths. Either way, knowing the functional forms for ψ_m and ψ_h is crucial. I therefore first review and assess several published expressions for ψ_m and ψ_h . The ψ_m and ψ_h functions from Paulson (1970), for example, are suitable for treating unstable stratification, and I discuss these no further. On the other hand, because the atmospheric surface layer over surfaces of ice or snow is often stably stratified, I focus on the forms of ψ_m and ψ_h in stable stratification, where there is little consensus on how to represent these.

2. Profile metrics

For investigating theoretical constraints on the behavior of the atmospheric surface layer profiles during stable stratification, using the gradient functions $\phi_m(\zeta)$ and $\phi_h(\zeta)$ is easier than using the profile functions $\psi_m(\zeta)$ and $\psi_h(\zeta)$. These gradient functions are related to the surface-layer profiles of wind speed, potential temperature, and specific humidity as (e.g., Dyer 1974)

$$\frac{dU}{dz} = \frac{u_*}{kz} \phi_m(\zeta), \quad (2.1a)$$

$$\frac{dT}{dz} = \frac{t_*}{kz} \phi_h(\zeta), \quad (2.1b)$$

$$\frac{dQ}{dz} = \frac{q_*}{kz} \phi_h(\zeta). \quad (2.1c)$$

Comparing (1.1) and (2.1), we get the expression that links the ψ and ϕ functions (e.g., Panofsky 1963):

$$\psi(\zeta) = \int_0^\zeta \frac{1 - \phi(\zeta')}{\zeta'} d\zeta'. \quad (2.2)$$

A host of ϕ_m and ϕ_h functions for stable stratification

(i.e., $\zeta > 0$) have been suggested. Of course, not all of these have proper theoretical behavior—some are simply empirical fits. Here I introduce four profile metrics to help us decide which ϕ_m and ϕ_h functions have proper behavior, especially in the limit of very stable stratification. These metrics are the gradient Richardson number Ri , the Deacon numbers for wind speed D_m and potential temperature D_h , and the turbulent Prandtl number Pr_t .

a. Gradient Richardson number

The gradient Richardson number is

$$Ri \equiv \frac{g}{T_v} \frac{dT/dz}{(dU/dz)^2}, \quad (2.3)$$

where g is the acceleration of gravity and T_v is the virtual temperature. From (2.1a) and (2.1b), we see that (2.3) can be written

$$Ri = \frac{g}{T_v} \frac{t_* k z}{u_*^2} \frac{\phi_h(\zeta)}{\phi_m^2(\zeta)}. \quad (2.4)$$

The group of variables in the front of (2.4) is just ζ , where

$$L = \frac{T_v u_*^2}{g k t_*}. \quad (2.5)$$

Consequently,

$$Ri = \frac{\zeta \phi_h(\zeta)}{\phi_m^2(\zeta)}. \quad (2.6)$$

Like ζ , the gradient Richardson number is a stratification parameter. In stable conditions, turbulence is presumed to cease and the flow becomes laminar when the Richardson number exceeds a critical value Ri_{cr} . Thus, we should expect accurate ϕ_m and ϕ_h functions to predict this critical value through (2.6). That is,

$$\lim_{\zeta \rightarrow \infty} Ri = Ri_{cr}. \quad (2.7)$$

Traditionally, Ri_{cr} is assumed to be 0.20–0.25 (Okamoto and Webb 1970; Busch 1973; Businger 1973; Nieuwstadt 1984). But Mahrt (1981) and Heinemann and Rose (1990) report that a larger value is sometimes indicated. Lyons et al. (1964) report nighttime data from Brookhaven, New York, that show “no clear ‘critical’ Richardson number” for Ri values up to at least 0.99 but also point out that these data do suggest the decreasing potential for turbulence for Ri greater than 0.25–0.50. Kondo et al. (1978) likewise report that turbulence can persist up to Ri values of 1 but conclude that the turbulence is only intermittent for Ri values between 0.2–0.3 and 1. Woods (1969) explained this apparent range in critical Richardson numbers somewhat differently by demonstrating how hysteresis can affect Ri_{cr} . He concluded that a turbulent flow becomes laminar when Ri exceeds 1, but a laminar flow does not

become turbulent until Ri falls below 0.25 (see also Plate 1971, p. 76). Canuto et al. (2001) partially corroborate this scenario by reporting that, in large-eddy and discrete numerical simulations, turbulence persists for Richardson numbers up to 1. In his observations at the South Pole, however, Lettau (1979) frequently found turbulence to exist even when Ri exceeded 1 and, thus, concluded that there is no critical Richardson number. Monin and Yaglom (1971, p. 440 f.) and Yamamoto (1975) also argue that no critical Richardson number seems to exist.

In light of this controversy, I conclude that the critical Richardson number for an existing turbulent flow is probably larger than the traditional value of 0.20 or 0.25; perhaps it is of order 1. Still, some have speculated that Ri does not reach a critical value at all: that turbulence does not cease as ζ increases.

b. Deacon numbers

Lettau (1957, 1979; see also Viswanadham 1979, 1982) uses two quantities to characterize profile curvature in the atmospheric surface layer, the Deacon numbers for wind speed (D_m) and potential temperature (D_h). Andreas (1998) also discusses these.

For wind speed,

$$D_m \equiv \frac{-z(d^2U/dz^2)}{dU/dz}. \quad (2.8)$$

From (2.1a), we easily see that

$$D_m(\zeta) = 1 - \frac{\zeta}{\phi_m(\zeta)} \frac{d\phi_m(\zeta)}{d\zeta}. \quad (2.9)$$

Similarly, for potential temperature,

$$D_h \equiv \frac{-z(d^2T/dz^2)}{dT/dz}, \quad (2.10)$$

and from (2.1b),

$$D_h(\zeta) = 1 - \frac{\zeta}{\phi_h(\zeta)} \frac{d\phi_h(\zeta)}{d\zeta}. \quad (2.11)$$

In neutral stratification, where $\zeta = 0$, D_m and D_h are both 1. As the stratification increases, however, reliable ϕ_m and ϕ_h functions should predict limiting D_m and D_h values that agree with theory and experiment. I will discuss theoretical limits for D_m and D_h as ζ gets large shortly, but the experimentally determined limits are inconclusive. For example, from profile observations at the South Pole, Lettau (1979) concludes that $D_m = 1/4$ and $D_h = -1/2$ in the limit of $\zeta \rightarrow \infty$. On the other hand, Viswanadham (1982) suggests that D_m is small but slightly positive; he gives 0.04 as the limit for D_m with increasing stratification. He did not evaluate D_h .

One reason for this absence of definitive results must surely be the difficulty in measuring second derivatives of U and T in the atmospheric surface layer. As a min-

imum, such measurements require four levels of well-calibrated sensors.

c. Turbulent Prandtl number

The turbulent Prandtl number is the ratio of the eddy diffusivities for momentum (K_m) and sensible heat (K_h). These fluxes are related to the respective wind speed and potential temperature gradients through these diffusivities (e.g., Dyer 1974):

$$\tau = \rho u_*^2 = \rho K_m \frac{dU}{dz}, \quad (2.12a)$$

$$H_s = -\rho c_p u_* t_* = -\rho c_p K_h \frac{dT}{dz}. \quad (2.12b)$$

From (2.1) and (2.12), we thus see that

$$K_m(\zeta) = u_* k z / \phi_m(\zeta), \quad (2.13a)$$

$$K_h(\zeta) = u_* k z / \phi_h(\zeta). \quad (2.13b)$$

As a result, the turbulent Prandtl number is

$$Pr_t(\zeta) \equiv \frac{K_m(\zeta)}{K_h(\zeta)} = \frac{\phi_h(\zeta)}{\phi_m(\zeta)}. \quad (2.14)$$

Much of the discussion regarding Pr_t has concentrated on its value at neutral stability, $\zeta = 0$ (e.g., Businger et al. 1971; Kader and Yaglom 1990; Höögström 1996). Again, since I am interested more in the behavior of the ϕ_m and ϕ_h functions in the limit of very stable stratification, I focus on the limit of $Pr_t(\zeta)$ as ζ gets large.

Because Pr_t contains the ratio ϕ_h/ϕ_m , as does Ri , if the Richardson number is unbounded as ζ increases, Pr_t could be too. Monin and Yaglom (1971, p. 440 f.) therefore believe that Pr_t increases without bound as ζ increases. Mahrt (1998) reaches essentially the same conclusion, explaining that pressure fluctuations in the atmosphere caused by gravity waves can transfer momentum but not sensible heat (cf. Beljaars and Holtslag 1991). Observations by Kim and Mahrt (1992) seem to substantiate this conclusion. Using aircraft data collected over Kansas and Oklahoma, they show Pr_t increasing without bound for Ri values up to almost 1. In contrast, Howell and Sun (1999) show surface-layer data from the Microfronts experiment in Kansas in 1995 for which the turbulent Prandtl number remains near 1 for ζ up to 10.

d. In laminar flow

As the stratification increases—that is, as ζ approaches infinity—a turbulent flow eventually becomes laminar, at least in a laboratory setting. Here molecular processes alone must support the fluxes of momentum and sensible heat. Thus, for the momentum flux, rather than (2.12a), we have (e.g., Tennekes and Lumley 1972, p. 160)

$$\tau = \rho u_*^2 = \rho \nu \frac{dU}{dz}, \tag{2.15}$$

where ν is the kinematic viscosity of air. As a result,

$$\lim_{\zeta \rightarrow \infty} \phi_m(\zeta) = \frac{u_* k z}{\nu} = \frac{u_* k L \zeta}{\nu}. \tag{2.16}$$

Likewise, the sensible heat flux in laminar flow is

$$H_s = -\rho c_p u_* t_* = -\rho c_p D \frac{dT}{dz}, \tag{2.17}$$

where D is the thermal diffusivity of air. Consequently,

$$\lim_{\zeta \rightarrow \infty} \phi_h(\zeta) = \frac{u_* k z}{D} = \frac{u_* k L \zeta}{D}. \tag{2.18}$$

Therefore, in the limit of laminar flow, the turbulent Prandtl number should obey

$$\lim_{\zeta \rightarrow \infty} \text{Pr}_t(\zeta) = \lim_{\zeta \rightarrow \infty} \frac{\phi_h(\zeta)}{\phi_m(\zeta)} = \frac{\nu}{D}, \tag{2.19}$$

which is the molecular Prandtl number, approximately 0.71 for air. Notice that, in this context, Pr_t is a bound quantity that is of order 1. Of course, this extension to laminar flow does not consider intermittent processes in the stable atmosphere, such as wave breaking, that can periodically destroy the laminar flow and foster momentum exchange with little heat transfer, as Monin and Yaglom (1971, p. 440 f.) and Mahrt (1998) explain.

From (2.16) and (2.18), we can also evaluate the Deacon numbers in the limit of laminar flow. From (2.9) and (2.16),

$$\lim_{\zeta \rightarrow \infty} D_m(\zeta) = 0; \tag{2.20}$$

and from (2.11) and (2.18),

$$\lim_{\zeta \rightarrow \infty} D_h(\zeta) = 0. \tag{2.21}$$

That is, both the wind speed and potential temperature profiles are linear in laminar flow and, thus, have no curvature. The respective Deacon numbers must therefore be zero.

In summary, these laminar limits are targets for $D_m(\zeta)$, $D_h(\zeta)$, and $\text{Pr}_t(\zeta)$ in the limit of very stable stratification. We realize though that contrary experimental and theoretical results call into question the idea of relying strictly on these laminar limits for flows in the atmospheric boundary layer. Nevertheless, real flows should not stray far from these laminar limits as the stratification increases.

3. A sampling of gradient functions for stable stratification

Dozens of expressions for the ϕ_m and ϕ_h functions have been published over the last 40 years. Dyer (1974), Yamamoto (1975), Yaglom (1977), and Sorbjan (1989,

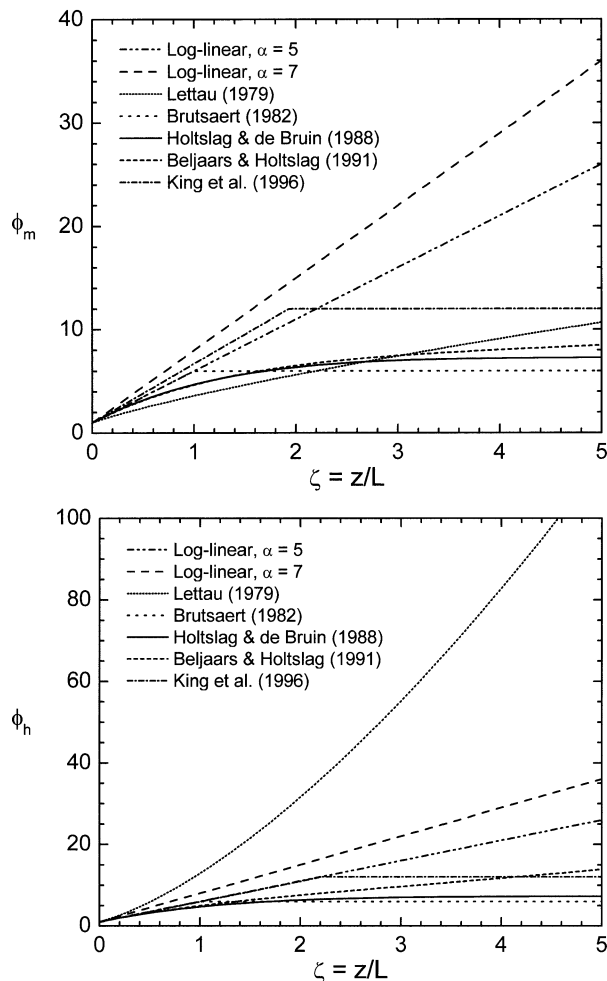


FIG. 1. A sampling of (top) ϕ_m and (bottom) ϕ_h functions for stable stratification.

p. 74 ff.), for example, summarize some of these functions. Since I cannot hope here to provide an encyclopedic review of all of these functions, I select for discussion a small sample of representative functions. Readers can evaluate other functions themselves with the techniques I will describe.

a. Log-linear

Classically, the log-linear relation,

$$\phi_m(\zeta) = \phi_h(\zeta) = 1 + \alpha \zeta, \tag{3.1}$$

is the usual model for ϕ_m and ϕ_h in stable stratification. The constant α is generally reported to be in the range from 5 (Webb 1970; Dyer 1974; Large and Pond 1981) to 7 (Wieringa 1980; Large and Pond 1982; Höglström 1988).

Figure 1 shows plots of ϕ_m and ϕ_h for α values of 5 and 7, while Table 1 lists the Deacon, gradient Richardson, and Prandtl numbers for these functions in the limit of large ζ . The Deacon and Prandtl numbers

TABLE 1. A comparison of the predictions of several sets of ϕ_m and ϕ_h functions in the limit of very stable stratification. The laminar case is a possible nonturbulent limit.

ϕ_m, ϕ_h	Lim $\zeta \rightarrow \infty$			
	D_m	D_h	Ri	Pr_t
Log-linear, $\alpha = 5$	0	0	$\frac{1}{5} = 0.20$	1
Log-linear, $\alpha = 7$	0	0	$\frac{1}{7} = 0.14$	1
Lettau (1979)	$\frac{1}{4}$	$-\frac{1}{2}$	ζ	$(4.5\zeta)^{3/4}$
Brutsaert (1982)	1	1	$\frac{\zeta}{6}$	1
Holtslag and de Bruin (1988)	0	0	1.43	1
Beljaars and Holtslag (1991)	0	$-\frac{1}{2}$	$\left(\frac{2}{3}\zeta\right)^{1/2}$	$\left(\frac{2}{3}\zeta\right)^{1/2}$
King et al. (1996)	1	1	$\frac{\zeta}{12}$	1
Laminar	0	0		$\frac{\nu}{D} \approx 0.71$

for these log-linear functions reach the proper laminar theoretical limits of 0 and order 1, respectively. The critical Richardson numbers implied by the $\alpha = 5$ and $\alpha = 7$ versions of the log-linear gradient functions, 1/5 and 1/7, respectively, are approximately in the classical range, 0.20–0.25. As I explained, however, these critical Richardson numbers are too small for atmospheric flows in light of more recent theory and observations.

b. Lettau

On the basis of his profile observations at the South Pole, Lettau (1979) introduced the following novel expressions for ϕ_m and ϕ_h :

$$\phi_m(\zeta) = (1 + 4.5\zeta)^{3/4}, \tag{3.2a}$$

$$\phi_h(\zeta) = (1 + 4.5\zeta)^{3/2}. \tag{3.2b}$$

Figure 1 depicts these functions. Lettau’s ϕ_h function predicts by far the steepest temperature gradient among any of the functions that I survey.

Table 1 lists the Deacon, Richardson, and Prandtl numbers that Lettau’s functions imply in the limit of large ζ . Lettau specifically formulated his ϕ_m and ϕ_h functions to produce the rather unusual D_m and D_h values of 1/4 and $-1/2$ because these values mirror the results of his profile observations at South Pole. His predicted Richardson number does not approach a limit

at large ζ but, rather, continues increasing in proportion to ζ . Likewise, his turbulent Prandtl number does not reach a laminar limit but increases as $\zeta^{3/4}$. As I mentioned above, some have speculated that such unbounded Richardson and Prandtl numbers could exist in an intermittently turbulent, stable boundary layer. None, however, have corroborated the steepness of Lettau’s ϕ_h function.

c. Brutsaert

Brutsaert (1982, p. 71) recommends the log-linear form for ϕ_m and ϕ_h but constrains these to values of 6 or less. That is,

$$\phi_m(\zeta) = \phi_h(\zeta) = 1 + 5\zeta \quad \text{for } 0 \leq \zeta \leq 1 \tag{3.3a}$$

$$\phi_m(\zeta) = \phi_h(\zeta) = 6 \quad \text{for } \zeta > 1. \tag{3.3b}$$

Kondo et al. (1978) also suggest that ϕ_m is limited by 6. Figure 1 shows plots of the functions in (3.3). At large ζ , they yield the smallest ϕ_m and ϕ_h values for any of the functions I am surveying.

Table 1 lists the Deacon, Richardson, and Prandtl numbers predicted by Brutsaert’s functions in the limit of large ζ . His functions predict rather unusual limiting Deacon numbers of $D_m = D_h = 1$. His functions also predict a Richardson number that is unbounded; it increases as $\zeta/6$. In other words, he predicts that no critical Richardson number exists. In a break with the other functions in Table 1 that predict an unbounded Richardson number [except those from King et al. (1996)], however, his functions predict that the turbulent Prandtl number reaches a limit of 1.

d. Holtslag and de Bruin

Holtslag and de Bruin (1988) build on analyses by Carson and Richards (1978) and Hicks (1976) to develop expressions for ϕ_m and ϕ_h that are specially adapted for very stable stratification (cf. Launiainen and Vihma 1990):

$$\begin{aligned} \phi_m(\zeta) &= \phi_h(\zeta) \\ &= 1 + 0.7\zeta \\ &\quad + 0.75\zeta(6 - 0.35\zeta) \exp(-0.35\zeta). \end{aligned} \tag{3.4}$$

Figure 1 shows plots of these functions. They are fairly close to Brutsaert’s (1982) in the plotted range but continue increasing slowly with ζ , while his functions are constant at 6 for ζ larger than 1.

Table 1 lists the limiting values of the Deacon, Richardson, and Prandtl numbers implied by the Holtslag and de Bruin functions. All these values reach reasonable limits as ζ increases. The Deacon numbers D_m and D_h both go to zero, the limit for laminar flow. The turbulent Prandtl number is always 1, which is the approximate order of the molecular Prandtl number. Finally, Holtslag and de Bruin’s functions predict that the

critical Richardson number is 1.43, in line with my earlier discussion that modern ideas suggest a critical Richardson number of order 1.

e. Beljaars and Holtslag

Beljaars and Holtslag (1991) suggest slightly altered versions of the ϕ_m and ϕ_h functions given by Holtslag and de Bruin (1988) because, presumably, these new functions “are more consistent with critical Ri considerations.” The Beljaars and Holtslag functions are

$$\phi_m(\zeta) = 1 + \zeta + \frac{2}{3}\zeta(6 - 0.35\zeta) \exp(-0.35\zeta), \quad (3.5a)$$

$$\begin{aligned} \phi_h(\zeta) = 1 + \zeta \left(1 + \frac{2}{3}\zeta \right)^{1/2} \\ + \frac{2}{3}\zeta(6 - 0.35\zeta) \exp(-0.35\zeta). \end{aligned} \quad (3.5b)$$

Figure 1 shows plots of these functions.

Table 1 lists the values of the Deacon, Richardson, and Prandtl numbers implied by Beljaars and Holtslag’s functions in the limit of large ζ . The limiting Deacon number for the wind speed profile, 0, agrees with the laminar limit. The Deacon number for the temperature profile, $-1/2$, on the other hand, does not; though it is the same as Lettau’s (1979) value. Beljaars and Holtslag’s functions also predict that no critical Richardson number exists; for their functions, Ri increases as $[(2/3)\zeta]^{1/2}$. Likewise, their predicted turbulent Prandtl number does not have a limiting value but also increases as $[(2/3)\zeta]^{1/2}$.

f. King et al.

King et al. (1996) take an approach similar to Brutsaert’s (1982), basing ϕ_m and ϕ_h on log–linear relations but limiting these functions to a maximum of 12. That is, their formulation is

$$\phi_m(\zeta) = 1 + 5.7\zeta, \quad \phi_m(\zeta) \leq 12, \quad (3.6a)$$

$$\phi_h(\zeta) = 0.95 + 4.99\zeta, \quad \phi_h(\zeta) \leq 12. \quad (3.6b)$$

Here the additive constants and the coefficients of the ζ terms come from King and Anderson’s (1994) profile measurements at Halley Station on the Antarctic continent. Figure 1 shows plots of these ϕ_m and ϕ_h functions.

Table 1 lists values for the profile metrics implied by the functions suggested by King et al. in the limit of large ζ . Both D_m and D_h equal 1 in very stable conditions, contrary to the predictions from laminar flow theory and at odds with all results except Brutsaert’s (1982). The King et al. functions also do not produce a critical Richardson number; in their formulation, Ri increases monotonically as $\zeta/12$. Notice that the King et al. functions are the only ones that I consider for

which the turbulent Prandtl number at $\zeta = 0$ is not 1; their functions imply $Pr_t = 0.95$ at neutral stability, in line with Höögström’s (1996) recent review. In very stable stratification, their predicted turbulent Prandtl number is 1, as predicted by several other sets of functions in Table 1.

g. Summary

We see from Fig. 1 that, for $0 \leq \zeta \leq 0.5$, where most profile data for evaluating the ϕ_m and ϕ_h functions have been collected, the seven candidate sets of functions show only minor differences. As the stratification increases, however, and the turbulence likely becomes intermittent, the ϕ_m and ϕ_h functions show diverging opinions. The two log–linear expressions for ϕ_m —which admittedly were never intended for extrapolating into very stable stratification—suggest very large values. The other five functions, which are intended explicitly for treating very stable stratification, imply ϕ_m values typically between 6 and 12.

For ϕ_h , again the log–linear functions imply very large values in very stable stratification but really should not be extrapolated into this region. Lettau’s (1979) function, in contrast, suggests even larger values and was formulated specially to treat very stable stratification. Nevertheless, it has no corroboration that I know of; I must thus assume it is unrealistically large. The other four ϕ_h functions in Fig. 1 typically predict values between 6 and 14 in very stable stratification.

I use the values of the four profile metrics, D_m , D_h , Ri, and Pr_t , in the limit of large ζ to judge which of these functions have realistic behavior. I eliminate the two log–linear sets immediately because they were never intended to treat very stable stratification. I eliminate Lettau’s (1979) functions because these imply the most unusual profile metrics of all the functions in Table 1 and because ϕ_h seems too large. Though mathematically simple, I also eliminate the Brutsaert (1982) and King et al. (1996) functions because of their implied Deacon numbers in the limit of large ζ .

Finally, I eliminate Beljaars and Holtslag’s (1991) functions because I have seen no hard evidence that turbulence persists without limit as the stratification increases. In particular, Howell and Sun’s (1999) Microfronts data do not show Ri increasing as rapidly with ζ as Beljaars and Holtslag’s functions predict and do not give Ri values larger than 0.6 for ζ up to 10. In other words, most analyses that have addressed the question suggest a critical Richardson number of order 1 exists. Likewise, Howell and Sun suggest the turbulent Prandtl number is also of order 1 in very stable stratification contrary to Beljaars and Holtslag’s prediction of no limiting Prandtl number.

The functions developed by Holtslag and de Bruin (1988) imply profile metrics that agree with these assessments and are thus the functions I recommend for representing stratification effects in surface-layer wind

speed, temperature, and humidity profiles in stable stratification. Launiainen (1995), Vihma (1995), and Jordan et al. (1999, 2001), among others, have also settled on these stability functions for treating stable stratification.

The radiative flux divergence in the atmospheric surface layer is a process that may affect the conclusions above. Although a full evaluation of this term in the heat budget of the atmospheric surface layer is beyond my scope, I want to raise the issue as an area that needs research. Briefly, near-surface water vapor absorbs and emits longwave radiation. Depending on the near-surface temperature and humidity profiles, this exchange may ruin the assumption that a surface layer exists in which the vertical flux of sensible heat is constant with height. In turn, the ϕ_h function especially would then not obey Monin–Obukhov similarity.

Normally, the radiative flux divergence is negligible. But in very stable stratification, when the winds are light and the magnitude of the sensible heat flux is small, the radiative flux divergence can lead to a significant variation in the sensible heat flux with height (e.g., Coantic and Seguin 1971). Coantic and Seguin (1971), Garratt and Brost (1981), and Narasimha and Vasudeva Murthy (1995), among others, investigated the effects of radiative flux divergence on atmospheric surface layer profiles but did not treat the specific cases of snow-covered surfaces or temperatures well below freezing, when the water vapor density in the atmospheric surface layer will be small. Hence, I cannot reliably infer what their results might say about the effects of the radiative flux divergence over surfaces of ice or snow. We need a thorough study of the possible interactions between turbulence and radiation in the atmospheric surface layer at temperatures well below freezing to evaluate whether these interactions can explain the variety of ϕ_m and ϕ_h functions reported in the literature.

4. Scalar roughness over snow and ice

Andreas (1987) built on the surface-renewal models of Brutsaert (1975) and Liu et al. (1979) to produce the only theoretically based model that specifically predicts z_T and z_Q over ice and snow-covered surfaces. Although I had scant data with which to test that model when I published it, sporadic tests have been published since (e.g., Munro 1989; Bintanja and Van den Broeke 1995). More importantly, since that model is the only one specifically for snow and ice surfaces, many have been using it for numerical modeling (e.g., Morris 1989; Launiainen and Cheng 1998; Jordan et al. 1999), though, to my mind, it has not been adequately validated.

The model's basic result is an equation that predicts the scalar roughness z_s from the roughness Reynolds number $R_* (=u_*z_0/\nu)$,

$$\ln(z_s/z_0) = b_0 + b_1(\ln R_*) + b_2(\ln R_*)^2, \quad (4.1)$$

TABLE 2. Values of the coefficients to use in (4.1) for estimating the scalar roughness lengths in the three aerodynamic regimes.

	$R_* \leq 0.135$ Smooth	$0.135 < R_* < 2.5$ Transition	$2.5 \leq R_* \leq 1000$ Rough
Temperature (z_T/z_0)			
b_0	1.250	0.149	0.317
b_1	0	-0.550	-0.565
b_2	0	0	-0.183
Humidity (z_Q/z_0)			
b_0	1.610	0.351	0.396
b_1	0	-0.628	-0.512
b_2	0	0	-0.180

where z_s is either z_T or z_Q . Table 2 lists the polynomial coefficients, b_0 , b_1 , and b_2 .

Comparing (4.1) and the coefficients summarized in Table 2, we see that (4.1) is a piecewise-continuous function with three pieces. For aerodynamically smooth flow, z_s/z_0 is independent of the roughness Reynolds number because here molecular effects control the exchange of both momentum and scalars. That is, both scale similarly with u_* . For aerodynamically rough flow, in contrast, the viscous boundary layer continually thins with increasing u_* , the surface roughness elements protrude farther above this layer, and pressure forces become more important in transferring momentum. The effect is that z_0 increases with u_* ; while z_s , which is still dictated by molecular processes, does not change as rapidly. Hence, z_s/z_0 is a monotonically decreasing function of R_* for aerodynamically rough flow. Andreas (1987) simply made a log–log interpolation between the limits of smooth and rough flow to fill in the transition region in Table 2.

I want to test this model here with several datasets that I have located or that have become available since Andreas (1987) appeared. Hicks and Martin (1972), Thorpe et al. (1973), Joffre (1982), King and Anderson (1994), and Calanca (2001) have all reported measurements of quantities related to z_T or z_Q ; but these are small datasets, or the reported data were not in a form that I could use.

The primary reason for the scanty data is the difficulty in making the required measurements. Analyses for z_T and z_Q rely on (1.3), but the fluxes H_s and H_L are generally smaller in magnitude in stable stratification than in unstable stratification and can be especially small over snow and ice surfaces. That is, often the magnitudes of H_s and H_L are comparable to the experimental uncertainty in the measurements of these values. Likewise, the required gradients in (1.3), $T_s - T(z)$, and $Q_s - Q(z)$, are often small with large experimental uncertainties. In total, then, over surfaces of snow and ice, experimental uncertainties can often swamp values of C_{Hz} and C_{Ez} calculated from (1.3) and, thus, values of z_T and z_Q calculated from (1.4). Still, I have located five datasets that are modestly sized and seem to have enough signal-to-noise ratio to provide estimates of z_T

and z_0 . For these sets, I was also usually able to obtain and analyze the raw data.

a. Munro's data

Munro (1989) measured profiles of wind speed and temperature at four levels between 0.25 and 1.00 m over the melting Peyto Glacier (Alberta, Canada; e.g., Goodison 1970). The value of this dataset is that the surface temperature is well known, 0°C , and the surface-air temperature difference is unusually large—sometimes as large as 12°C .

Munro's original paper contains his analysis of z_T/z_0 as a function of R_* , but almost all of his plotted values are above the line set by (4.1). To obtain his results, however, Munro used the log-linear form for ϕ_m and ϕ_h with $\alpha = 5$; assumed $k = 0.41$; and most importantly, modified each of his wind speed and temperature profile heights by adding 0.17 m to each original height. He evidently based this 0.17-m correction on the typical trough-to-peak height of the microtopography of the glacier and what he viewed as ambiguity in his zero-reference height.

I have three concerns with these manipulations. That 0.17 m seems akin to a displacement height, but displacement heights are always *subtracted* from the measured height. I am not sure what adding 0.17 m to the height means physically. Second, because momentum can be transferred by pressure forces acting on the roughness elements, Thom (1971) interpreted the displacement height as the height at which the roughness elements absorb momentum. Because pressure forces do not transfer heat, however, it seems unlikely that the temperature profile should exhibit the same displacement height as the wind speed profile, as Munro acknowledges himself. Finally, Andreas (1995) adapted a form-drag model developed by Raupach (1992) to investigate momentum transfer over a surface covered with sastrugi—that is, over a fairly rough surface like that of the Peyto Glacier. I infer from this modeling that the ratio of displacement height to the height of the roughness elements is much less than one. Consequently, Munro's choice of 0.17 m seems too large by a factor of, at least, three. The upshot is that, since Munro's measurement heights were 0.25, 0.50, 0.75, and 1.00 m, adding 0.17 m to each height causes significant changes in the apparent curvature of the profiles and could easily explain the difference between his results and the Andreas (1987) model.

I therefore obtained Munro's raw profile data (S. Munro 1995, personal communication) and analyzed these myself to estimate z_T and z_0 . This analysis simply involved fitting his wind speed and potential temperature profile data iteratively with (1.1a) and (1.1b). This fitting yields u_* , t_* , and L . Since $U(z_0) = 0$, (1.1a) then gives z_0 ; and since $T(z_T) = T_s = 0^\circ\text{C}$, (1.1b) gives z_T . Unlike Munro, I assumed no displacement height; set k

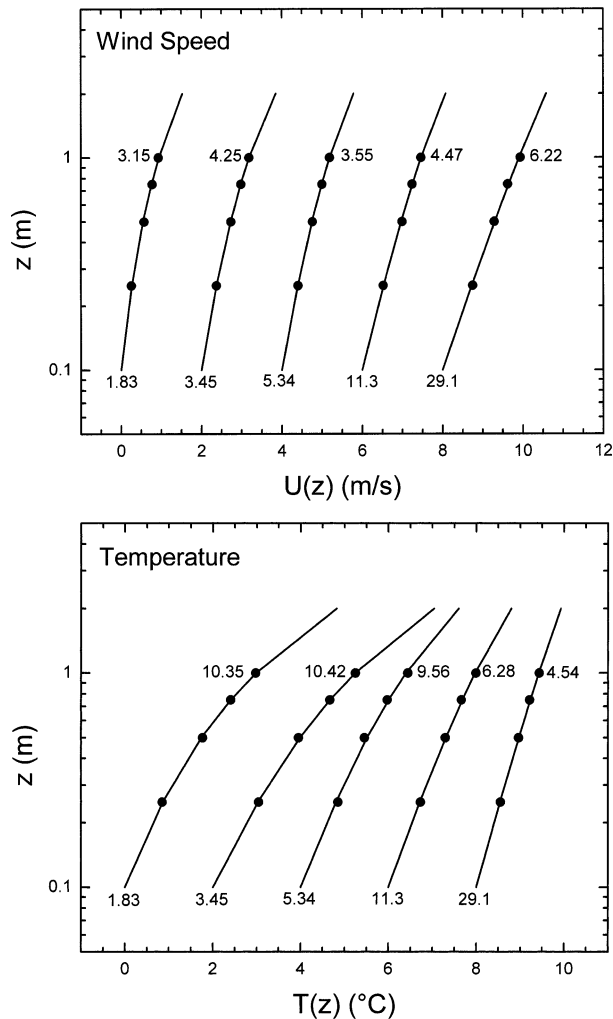


FIG. 2. Five typical (top) wind speed and (bottom) potential temperature profiles from Munro's (1989) dataset. In each panel, the markers show the data, and the lines are the fits based on (1.1a) and (1.1b) using the Holtslag and de Bruin (1988) stability corrections. The horizontal scale is relative rather than absolute. In the wind speed plot, the number at $z = 1$ m gives the measured wind speed (in m s^{-1}) at 1 m; in the temperature plot, the number at $z = 1$ m gives the potential temperature (in $^\circ\text{C}$) there. The number under each profile is the Obukhov length in meters.

$= 0.40$; and on the basis of the last section, used the Holtslag and de Bruin (1988) functions for ψ_m and ψ_h .

Figure 2 demonstrates the success of this fitting with five representative pairs of wind speed and potential temperature profiles. In each panel, the left profile is the second most stable run in the dataset; the right profile is the one nearest neutral stratification. The three middle profiles get more nearly neutral from left to right. The correlation coefficients of the fits depicted in Fig. 2 are all at least 0.997. Of the 122 pairs of Munro's profiles that I analyzed, the smallest correlation coefficient for my fitting was 0.996. Figure 2 and these correlation coefficients are testimony to my choice of the Holtslag and de Bruin (1988) stability corrections and to my

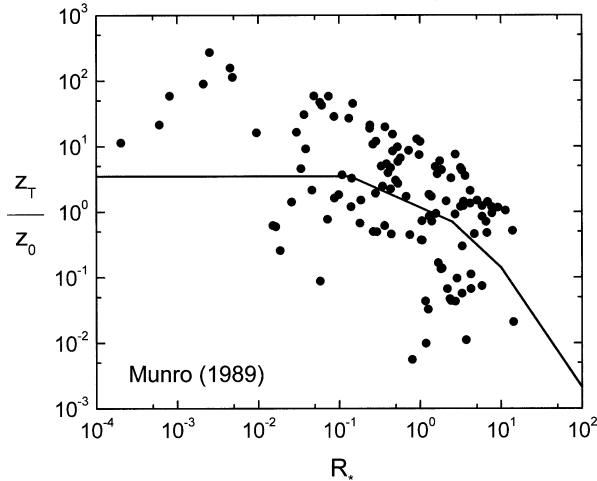


FIG. 3. The ratio z_T/z_0 as a function of the roughness Reynolds number R_* based on my reanalysis of Munro's (1989) profile data collected over the Peyto Glacier. The line is the Andreas (1987) model, (4.1).

decision to ignore Munro's suggestion that a displacement height is necessary.

Figure 3 compares my results from this reanalysis with the Andreas (1987) model for z_T/z_0 . Plots of z_s/z_0 are common in this business because this quantity lets us estimate the neutral-stability scalar transfer coefficient at reference height z (i.e., C_{sNz}) without the added steps of calculating z_s and z_0 individually. That is, from (1.4a) with $\zeta = 0$ (cf. Garratt and Hicks 1973),

$$C_{sNz} = \frac{C_{DNz}}{1 - k^{-1} C_{DNz}^{1/2} \ln(z_s/z_0)}. \quad (4.2)$$

Here, C_{DNz} is the neutral-stability drag coefficient at z (e.g., Andreas 1998),

$$C_{DNz} = \frac{k^2}{[\ln(z/z_0)]^2}. \quad (4.3)$$

The data and the model in Fig. 3 seem to agree startlingly well, both with respect to magnitude and to R_* dependence. In particular, the data and the model agree much better than in Munro's (1989) original analysis.

Careful readers will realize, however, that z_0 appears in both the dependent and independent variables in Fig. 3. This shared variable could thus lead to an artificially good (or bad) correlation. And, as I explain in the appendix, Fig. 3 apparently does suffer from this effect: The artificial correlation seems to explain the tendency for z_T/z_0 to decrease with increasing R_* at approximately the same rate as the model predicts. Consequently, I hesitate to conclude that Fig. 3 confirms the predicted R_* dependence in z_T/z_0 . The artificial correlation, on the other hand, has no influence on the typical magnitude of the z_T/z_0 values, which the model predicts well for R_* between 0.1 and 10.

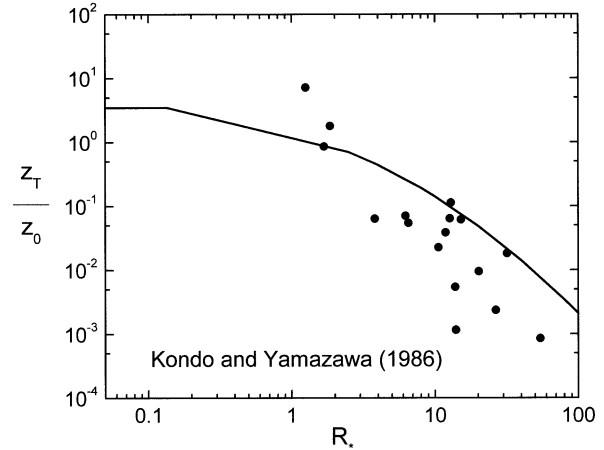


FIG. 4. The ratio z_T/z_0 as a function of the roughness Reynolds number R_* based on my calculations using the Kondo and Yamazawa (1986) data, which were collected over snow-covered ground. The line is the Andreas (1987) model, (4.1).

b. Kondo and Yamazawa's data

Kondo and Yamazawa (1986) report measurements of the wind speed and temperature profiles at six levels over snow-covered ground in Japan. Using a profile analysis like the one I just described, they obtained from these profiles u_* , L , C_{DN1} , and C_{HN1} —the latter two being neutral-stability values of the drag coefficient and the sensible heat transfer coefficient at a reference height of 1 m. Although their paper shows plots of some of these quantities, the details were not sufficient for my reanalysis. But J. Kondo (1986, personal communication) kindly provided me a table of their entire u_* , L , C_{DN1} , and C_{HN1} dataset. I earlier converted these C_{DN1} and C_{HN1} values to C_{HN10} (i.e., a 10-m reference height) and compared these with the model predictions in Andreas (1987). Here I further convert these tabulated values to z_T , z_0 , and R_* .

From (1.4a), we see that, for a 1-m reference height, at neutral stability,

$$C_{HN1} = \frac{k^2}{[\ln(1/z_0)][\ln(1/z_T)]}. \quad (4.4)$$

Analogously, the neutral-stability drag coefficient for a height of 1 m is just (4.3) with $z = 1$ m. Thus, from the values tabulated in the Kondo and Yamazawa dataset, I could easily compute z_0 , z_T , and R_* .

Figure 4 compares my calculations of z_T/z_0 and R_* from the Kondo and Yamazawa dataset with the Andreas (1987) model. Only three of the markers here reflect unstable stratification; all the other runs were made in stable stratification, though the stratification was never very strong. The data are generally within an order of magnitude of the model but, contrary to Fig. 3, tend to suggest values lower than the model. Although I have not confirmed this as I did with Fig. 3, the trend in z_T/z_0 with R_* probably reflects some self-correlation because of the shared z_0 .

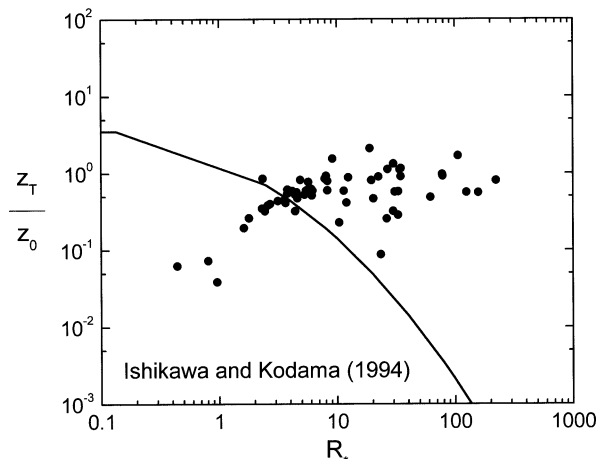


FIG. 5. The ratio z_T/z_0 as a function of the roughness Reynolds number R_* based on my reanalysis of Ishikawa and Kodama's (1994) data, which were collected over snow-covered ground. The line is the Andreas (1987) model, (4.1).

c. Ishikawa and Kodama's data

Ishikawa and Kodama (1994) report other profile and flux measurements over snow-covered ground in Japan. N. Ishikawa (1995, personal communication) kindly provided me all their raw data so I could reanalyze them for z_0 , z_T , u_* , and L .

Ishikawa and Kodama measured H_s with a sonic anemometer/thermometer. They also measured the snow-surface temperature, which was usually very near 0°C , and the temperature at a height of 1 m. From (1.3a) we see that these measurements provide C_{H1} , the sensible heat transfer coefficient appropriate at a reference height of 1 m.

The Ishikawa and Kodama dataset also includes measurements of the wind speed U at heights z_1 and z_2 —either 1 and 5 m or 0.1 and 1 m. From (1.1a), I could relate these measurements to u_* ; that is,

$$u_* = \frac{k[U(z_2) - U(z_1)]}{\ln(z_2/z_1) - \psi_m(z_2/L) + \psi_m(z_1/L)}. \quad (4.5)$$

Once this equation yields u_* , I could use (1.1a) to compute z_0 . Substituting this z_0 value and C_{H1} into (1.4a) let me also calculate z_T . Of course, these computations are iterative because L depends on u_* and the measured sensible heat flux. I again used the Holtslag and de Bruin (1988) functions for ψ_m and ψ_h in (1.4a) and (4.5). All of Ishikawa and Kodama's data were collected in stable stratification.

Figure 5 shows the results of my reanalysis of the Ishikawa and Kodama data. Although the centroid of the data cloud agrees fairly well with the model's predictions, the trend in the data with R_* is contrary to the model. I attribute this difference to the need to use (4.5) to evaluate u_* . Winds in this dataset were very light: The highest extrapolated 10-m wind speed for the data points plotted in Fig. 5 was 4.5 m s^{-1} , and most values

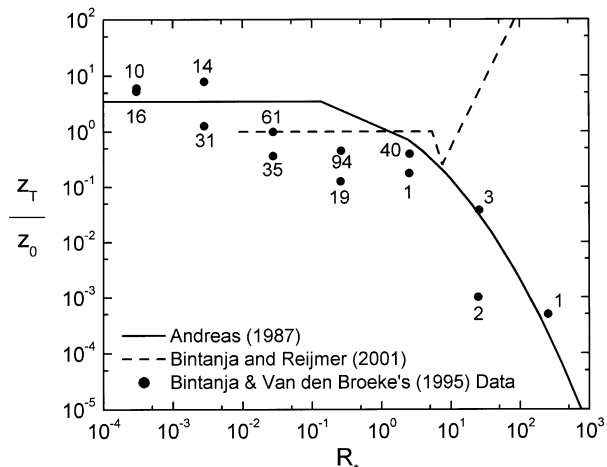


FIG. 6. The ratio z_T/z_0 as a function of the roughness Reynolds number R_* adapted from Bintanja and Van den Broeke (1995). The Bintanja and Van den Broeke measurements were over snow-covered and bare glacier ice in Antarctica. The number near each data marker represents the number of hourly averaged runs used to create the bin-average shown. The lines are Andreas's (1987) model, (4.1), and Bintanja and Reijmer's (2001) model, derived from (4.7).

were between 1 and 3 m s^{-1} . As a result, the difference in wind speed, $U(z_2) - U(z_1)$, in (4.5) was often small; the consequent large relative uncertainty in that difference therefore made the u_* evaluation imprecise. In fact, in creating Fig. 5, I eliminated 62 runs that had implied 10-m wind speeds less than 1 m s^{-1} . These runs with light winds led to unrealistically large z_0 and R_* values.

d. Bintanja and Van den Broeke's results

Bintanja and Van den Broeke (1995) report two-level measurements of wind speed and temperature at several sites over snow-covered and bare glacial ice near the Swedish station Svea in Queen Maud Land, Antarctica. They used a profile analysis, again based on (1.1a) and (1.1b), to evaluate z_0 , z_T , u_* , and thus R_* from these data. Their paper contains a plot of B_H^{-1} values bin-averaged in R_* bins, where (e.g., Garratt and Hicks 1973)

$$B_H^{-1} = \frac{1}{k} \ln\left(\frac{z_0}{z_T}\right). \quad (4.6)$$

I digitized this plot and converted the averaged B_H^{-1} values to z_T/z_0 averages.

Figure 6 shows my replottting of the Bintanja and Van den Broeke results. This plot represents many hours of data over a wide R_* range and is thus a valuable test of the Andreas (1987) model. The data in Fig. 6 do seem to corroborate the model—both with respect to the magnitude of z_T/z_0 and the trend in this ratio with R_* . All but three of the data markers in Fig. 6 are within half an order of magnitude of the model's predictions.

e. Bintanja and Reijmer's results

Bintanja and Reijmer (2001) report recent measurements of z_0 , z_T , and z_Q in the vicinity of Svea. They based their analysis on five-level profiles of wind speed, temperature, and specific humidity measured between 0.4 and 10 m above the surface. They restricted their analysis to cases of blowing and drifting snow, when u_* is above a threshold of 0.30 m s^{-1} , and deduced z_0 , z_T , and z_Q by fitting the profiles with semilogarithmic functions. That is, they made no corrections for the curvature in the semilogarithmic profiles caused by stratification and modeled by the ψ_m and ψ_h functions in (1.1).

They summarize their results as functions of u_* : for $u_* \leq 0.30 \text{ m s}^{-1}$,

$$z_0 = z_T = z_Q = 2 \times 10^{-4} \text{ m}; \quad (4.7a)$$

for $u_* > 0.30 \text{ m s}^{-1}$,

$$z_0 = 0.0039202u_*^{2.1968}, \quad (4.7b)$$

$$z_T = 14.302u_*^{10.144}, \quad (4.7c)$$

$$z_Q = 0.50324u_*^{6.1141}. \quad (4.7d)$$

In all of these, the roughness lengths are in meters for u_* in m s^{-1} .

The approximate quadratic dependence of z_0 on u_* in (4.7b) is in line with earlier assessments of how z_0 should behave in drifting and blowing snow (e.g., Owen 1964; Chamberlain 1983; Andreas and Claffey 1995). But the large exponents of the u_* terms in (4.7c) and (4.7d) imply that both z_T and z_Q get much larger than z_0 at large R_* , a result not supported by any theory or by any other data.

As an example of (4.7), I include in Fig. 6 the relation for z_T/z_0 as a function of R_* that (4.7) implies. Although this new model is not unreasonable for R_* less than 5, for larger R_* , Bintanja and Reijmer's model does not fit Bintanja and Van den Broeke's (1995) data.

f. Barry and Munn's data

The only dataset of even modest size that I have found suitable for my reanalysis and that has anything to say about z_Q over snow or ice is Barry and Munn's (1967). They released tritiated water vapor at the surface or at a height of 10 m over snow-covered ground in Chalk River, Ontario, Canada. Using radioactivity detection techniques, they measured the downwind water vapor concentration at a height of 0.3 m 45–90 m from the release point and could estimate the surface water vapor flux from a time series of snow-surface samples. They also measured the mean wind speed at five heights between 0.25 and 2 m and could therefore estimate u_* and z_0 . Their tabulated data include R_* and enough other information for me to estimate z_Q/z_0 . Figure 7 shows the results for their highest-quality runs.

Figure 7 also shows Andreas's (1987) model for z_Q/z_0

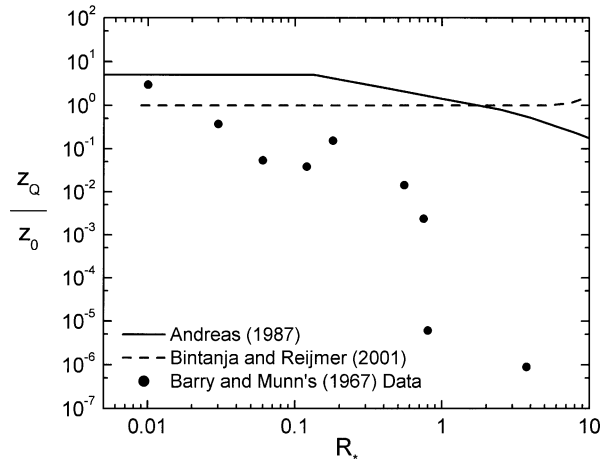


FIG. 7. The ratio z_Q/z_0 as a function of the roughness Reynolds number R_* based on the data obtained by Barry and Munn (1967) over snow-covered ground. The lines are Andreas's (1987) model, (4.1), and Bintanja and Reijmer's (2001) model, derived from (4.7).

and Bintanja and Reijmer's (2001) prediction of the same quantity based on (4.7). The data in Fig. 7 tend to be significantly below both model predictions. The z_Q/z_0 data do, however, decrease with increasing R_* as the Andreas model predicts—a distinct contrast between it and Bintanja and Reijmer's results. Still, Fig. 7 is inconclusive and thus implies that we have more work to do in evaluating z_Q .

Though Barry and Munn's is the only dataset I could find for this review, it is far from ideal. Because of their experimental design, I suspect their data suffer from nonstationarity and the horizontal inhomogeneity of their site. They also made no corrections for stratification in their analysis of the wind speed profiles (e.g., see Fig. 2), an omission that could have had a large effect on their u_* and z_0 values. In summary, though Barry and Munn's work was impressive for its time, I have enough doubts about their data that I present Fig. 7 primarily for its historical value and to motivate further work.

5. Discussion

Bin-averaging often clarifies relationship in plots of wildly scattered data. Therefore, following the example of Bintanja and Van den Broeke (1995) (Fig. 6), I bin-averaged the individual z_T/z_0 and R_* values in the Munro (Fig. 3), Kondo and Yamazawa (Fig. 4), and Ishikawa and Kodama (Fig. 5) datasets to see if such averaging gives a better picture of the R_* dependence in z_T/z_0 . To be faithful to the depictions in these plots, my averaging was geometric rather than arithmetic. That is, for both z_T/z_0 and R_* , I calculated the average of the logarithms of the values.

I identified just two R_* bins in the Munro data in Fig. 3: R_* values less than 0.01, and R_* values greater than 0.01. Likewise, I used just two bins in averaging the

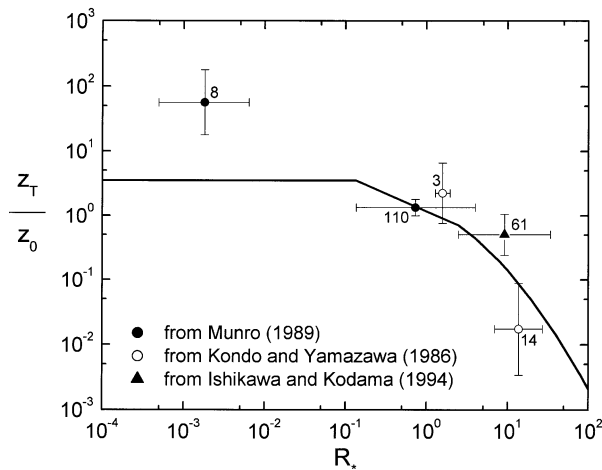


FIG. 8. Values of z_T/z_0 averaged in R_* bins for the Munro (Fig. 3), Kondo and Yamazawa (Fig. 4), and Ishikawa and Kodama (Fig. 5) datasets. The error bars are one std dev; the number beside each data marker gives the number of individual values used to create the average. The line is the Andreas (1987) model, (4.1).

Kondo and Yamazawa data in Fig. 4. The cluster of three points with R_* values between 1 and 2 are in one bin; all other points are in the second bin. Because the Ishikawa and Kodama data in Fig. 5 do not show much variation in z_T/z_0 with R_* , I lumped all these data in a single bin.

Figure 8 shows the results from this bin-averaging. The four points with R_* values between 0.7 and 20 that represent most of the data agree quite well with the model—both with respect to magnitude and to R_* dependence. The point in the aerodynamically smooth regime (below $R_* = 0.135$) suggests the model's predictions may be low here. But measuring in such light winds is often difficult, so eight points obtained in difficult experimental conditions may be suggestive but are not sufficient to refute the model. Besides, the more extensive dataset from Bintanja and Van den Broeke (Fig. 6) does not corroborate this discrepancy between the model and the measurements at small R_* . In fact, Figs. 6 and 8 now provide fairly strong support for the Andreas (1987) model for z_T/z_0 over the R_* range from 10^{-4} to 100.

One caveat in this conclusion, though, is that most of the z_T data that I have reviewed were collected in fairly warm conditions where snow would not have been blowing or drifting. The Bintanja and Van den Broeke (1995) set is the one exception. The issue is that Bintanja and Reijmer (2001) suggest that both z_T/z_0 and z_Q/z_0 increase with R_* when snow is drifting. My analyses here have not shown this effect, however. In particular, the Bintanja and Van den Broeke set, Fig. 6, which likely included drifting snow during the measurements with the large R_* values, does not substantiate Bintanja and Reijmer's empirical expressions for z_T and z_0 in drifting snow.

6. Conclusions

This review of current procedures for estimating the fluxes of sensible and latent heat over surfaces of snow and ice leads to some recommendations. First, because the atmospheric surface layer over snow and ice is often stably stratified, we need to reach some consensus on which functions, ψ_m and ψ_h , to use to model this stratification. On defining four profile metrics—the critical Richardson number, the Deacon numbers for wind speed and temperature, and the turbulent Prandtl number—I reviewed probable values for these in the limit of very stable stratification. Observations and theory suggest that Ri_{cr} and Pr_t are both bounded and of order 1, while D_m and D_h are approximately 0. Of the ψ_m and ψ_h functions that I reviewed here, the set that Holtslag and de Bruin (1988) developed satisfies these limits best. I recommend these functions for handling stable stratification in general and for treating stable stratification over snow and ice in particular.

The Andreas (1987) model is the only one specifically adapted to predict the scalar roughness lengths z_T and z_Q over snow and ice; though to date, it has had only sporadic and incomplete testing. Here I have reanalyzed five datasets collected over snow and ice for the explicit purpose of testing this model. My comparison of the z_Q results with the model in Fig. 7 is inconclusive because of presumed shortcomings in the data and, therefore, highlights the difficulty in measuring z_Q at low temperatures. For intellectual reasons and because of the technical challenges, we need to concentrate on making the measurements required for evaluating z_Q .

The other four datasets (Figs. 3–6), in contrast, agree fairly well with the model's predictions for z_T/z_0 . Since the model's independent variable, $R_* = u_* z_0 / \nu$, also contains z_0 , however, plots of z_T/z_0 versus R_* may suffer from fictitious correlation. In the appendix, I demonstrate that this self-correlation indeed affected the shape of the plot for Munro's (1989) data (Fig. 3). The implied correlation between z_T/z_0 and R_* , even if z_T were not related to any other variable, coincides closely with the model's predicted dependence for z_T/z_0 on R_* . This means that making scatterplots from individual datasets may not be a reliable way to judge a model's veracity.

Comparing data from various sources, however, at least mitigates the effects of bias errors in individual datasets. My bin-averaging of the Munro (1989), Kondo and Yamazawa (1986), and Ishikawa and Kodama (1994) datasets yielded data points that generally agree both in magnitude and in R_* dependence with the Andreas (1987) model (Fig. 8). This summary plot and the Bintanja and Van den Broeke (1995) results (Fig. 6) therefore finally provide fairly strong support for the Andreas model's predictions for z_T/z_0 for R_* values between 10^{-4} and 100.

Although I have been unable to similarly test the z_Q model directly, the success of (4.1) in representing the z_T/z_0 data supports it indirectly. Equation (4.1) is theo-

retically based; consequently, Figs. 6 and 8 essentially support that theory for heat transfer. Because most evidence from the atmospheric surface layer suggests that heat and moisture are transferred by similar processes, we can presume that the theory applies equally well for moisture transfer. Consequently, until we learn differently, (4.1) with the appropriate coefficients for humidity from Table 2 is also a reasonable model to use for predicting z_Q/z_0 .

The Andreas (1987) model for z_T/z_0 and z_Q/z_0 contains nothing that makes it specific for snow and ice surfaces. Only the parameterization for z_0 from Banke et al. (1980) that enabled me to predict C_H and C_E [i.e., see (1.4), (4.2), or (4.4)] limited it to use over snow and ice. In other words, the model's predictions for z_s/z_0 should be just as valid for other solid surfaces with small roughness elements—such as sand, bare soil, or mud flats—as they are for snow and ice.

Acknowledgments. This work would not have been possible if Junsei Kondo, Scott Munro, and Nobuyoshi Ishikawa had not generously sent me their datasets. I would also like to thank the three reviewers for helpful comments. The U.S. Department of the Army supported this work through Project 4A1611AT24; the U.S. National Science Foundation supported it with Awards OPP-98-14024 and OPP-00-84190.

APPENDIX

Self-Correlation in z_s/z_0 -versus- R_* Plots

Figures 3–7 show plots of $\log(z_s/z_0)$ versus $\log(R_*)$. The trends in the data in these plots could result from fictitious correlation because of the shared variable z_0 (e.g., Hicks 1978; Kenney 1982). Using ideas from Hicks (1978), I look at this question.

Figures 3–7 suggest that a reasonable model for the data summarized in these plots is

$$\ln(z_s/z_0) = a \ln R_* + b. \tag{A.1}$$

Let me define

$$Y \equiv \ln(z_s/z_0) = \ln z_s - \ln z_0 \quad \text{and} \tag{A.2}$$

$$X \equiv \ln R_* = \ln u_* + \ln z_0 - \ln \nu. \tag{A.3}$$

The correlation coefficient for the X and Y values is

$$\rho = \frac{\text{cov}(X, Y)}{s_X s_Y}, \tag{A.4}$$

where $\text{cov}(X, Y)$ is the X – Y covariance and s_X and s_Y are the sample standard deviations of X and Y . Likewise, the slope a and intercept b in (A.1) are

$$a = \frac{\text{cov}(X, Y)}{s_X^2} \quad \text{and} \tag{A.5}$$

$$b = \bar{Y} - a\bar{X}, \tag{A.6}$$

where \bar{X} and \bar{Y} are the sample averages of the X and Y values. That is,

$$\bar{X} = \overline{\ln u_*} + \overline{\ln z_0} - \overline{\ln \nu} \quad \text{and} \tag{A.7}$$

$$\bar{Y} = \overline{\ln z_s} - \overline{\ln z_0}, \tag{A.8}$$

where an overbar denotes the sample average.

We can evaluate the effects of the fictitious correlation on ρ , a , and b analytically by assuming that z_s , z_0 , u_* , and ν are all uncorrelated. For example, from the definition of the sample standard deviation, where N is the sample size,

$$s_X^2 = \frac{1}{N-1} \sum_{i=1}^N (X_i - \bar{X})^2, \quad \text{or} \tag{A.9}$$

$$s_X^2 = \frac{1}{N-1} \sum_{i=1}^N [(\ln u_{*i} + \ln z_{0i} - \ln \nu_i) - (\overline{\ln u_*} + \overline{\ln z_0} - \overline{\ln \nu})]^2. \tag{A.10}$$

Here, i is the index for the sample.

Because u_* , z_0 , and ν are all assumed to be uncorrelated for this analysis, from (A.10) we get

$$s_X^2 = s_{\ln u_*}^2 + s_{\ln z_0}^2 + s_{\ln \nu}^2, \tag{A.11}$$

where the terms on the right are the sample variances of $\ln u_*$, $\ln z_0$, and $\ln \nu$. Similarly,

$$s_Y^2 = s_{\ln z_s}^2 + s_{\ln z_0}^2, \tag{A.12}$$

where $s_{\ln z_s}^2$ is the sample variance of $\ln z_s$.

The X – Y covariance can be evaluated similarly:

$$\text{cov}(X, Y) = \frac{1}{N-1} \sum_{i=1}^N (X_i - \bar{X})(Y_i - \bar{Y}) \tag{A.13}$$

$$= \frac{1}{N-1} \sum_{i=1}^N \times [(\ln u_{*i} - \overline{\ln u_*}) + (\ln z_{0i} - \overline{\ln z_0}) - (\ln \nu_i - \overline{\ln \nu})] \times [(\ln z_{si} - \overline{\ln z_s}) - (\ln z_{0i} - \overline{\ln z_0})]. \tag{A.14}$$

Thus, under the assumption that all the variables are uncorrelated, the only covariance between z_s/z_0 and R_* results because of the shared variable z_0 :

$$\text{cov}(X, Y) = -s_{\ln z_0}^2. \tag{A.15}$$

That is, interestingly, the fictitious covariance of the logarithms of the nondimensional variables is equal to the negative of the variance of the log of the shared variable.

From (A.4), (A.11), (A.12), and (A.15), we consequently see that

$$\rho = \frac{-s_{\ln z_0}^2}{[(s_{\ln u_*}^2 + s_{\ln z_0}^2 + s_{\ln \nu}^2)(s_{\ln z_s}^2 + s_{\ln z_0}^2)]^{1/2}}. \tag{A.16}$$

That is, the correlation between $\ln(z_s/z_0)$ and $\ln R_*$ is always negative if it results strictly because of the shared

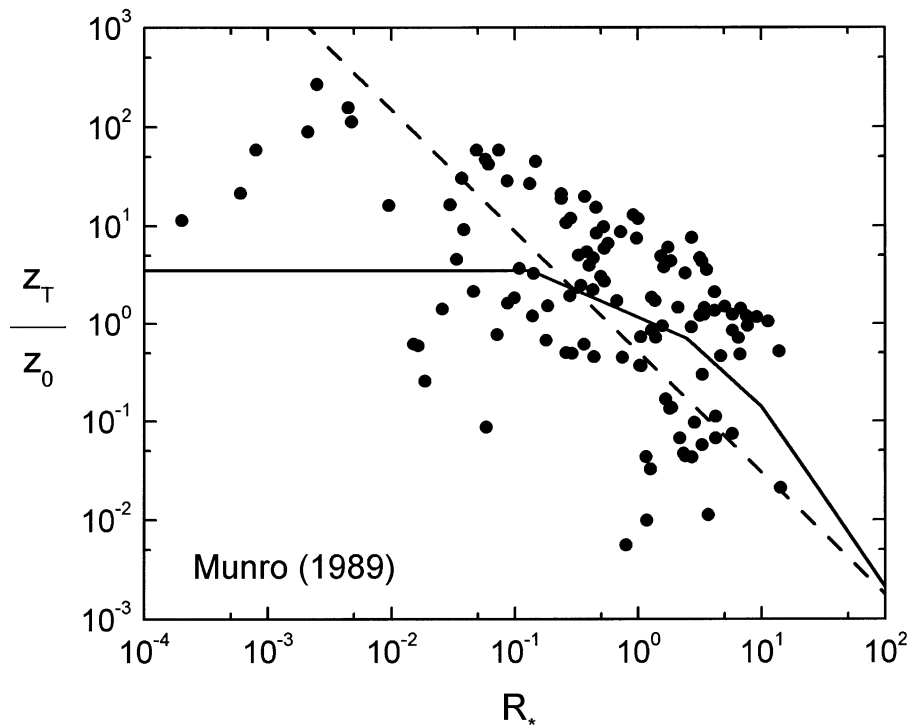


FIG. A1. Same as Fig. 3 but here the dashed line shows the least squares fit required by the presence of z_0 in both the dependent and independent variables.

z_0 . From (A.5), (A.11), and (A.15), we likewise get for the slope of the artificially correlated variables

$$a = \frac{-s_{\ln z_0}^2}{s_{\ln u_*}^2 + s_{\ln z_0}^2 + s_{\ln v}^2}, \tag{A.17}$$

which is again always negative. Finally, we can calculate b from (A.6)–(A.8) and (A.17).

Least squares linear regression, on which the above analysis is based, implicitly assumes that the X values are known perfectly and that the only uncertainty is in the Y values. This assumption is rarely true in geophysical data series and is certainly not true of our R_* values. Consequently, I like to also fit X versus Y with a least squares line and take the bisector of the two fitting lines as the “best” fit.

That is, the second step to this analysis is to fit the data as

$$X = a'Y + b'. \tag{A.18}$$

From (A.4), we see that the correlation coefficient for the X -versus- Y data is the same as for the Y -versus- X data. From (A.5), we can also immediately write

$$a' = \frac{\text{cov}(X, Y)}{s_Y^2}. \tag{A.19}$$

Hence, from (A.12) and (A.15),

$$a' = \frac{-s_{\ln z_0}^2}{s_{\ln z_s}^2 + s_{\ln z_0}^2}. \tag{A.20}$$

Finding the bisector of (A.1) and (A.18) is easier if we write (A.18) as

$$Y = \frac{1}{a'}X - \frac{b'}{a'}. \tag{A.21}$$

Then the bisector has an equation like (A.1) and (A.21),

$$Y = \hat{a}X + \hat{b}. \tag{A.22}$$

The slope of this bisector is

$$\hat{a} = \tan \left\{ 0.5 \left[\arctan(a) + \arctan\left(\frac{1}{a'}\right) \right] \right\}, \tag{A.23}$$

and its intercept is

$$\hat{b} = \bar{Y} - \hat{a}\bar{X}. \tag{A.24}$$

I have tested the effects of this self-correlation by evaluating ρ , \hat{a} , and \hat{b} for Munro’s (1989) dataset (see Fig. 3). Figure A1 shows the discouraging result.

Because the range of u_* values in the Munro (1989) dataset is small and because $s_{\ln z_0}$ and $s_{\ln z_T}$ are comparable, (A.16) shows that

$$\rho \approx \frac{-s_{\ln z_0}^2}{(2s_{\ln z_0}^2)^{1/2}} \approx -0.7; \tag{A.25}$$

(A.17) and (A.20) likewise suggest that the predicted slope, \hat{a} , is between -1 and -2 . That is, even if z_T is not correlated with anything, because of the shared z_0 , the correlation between $\ln(z_T/z_0)$ and $\ln R_*$ is still high

and the implied slope is similar to the slope that both the data and the model display. The dashed line in Fig. A1 shows the regression line (A.22) that results solely from this fictitious correlation.

In summary, at least for the Munro (1989) dataset, the fictitious correlation between the z_T/z_0 and R_* values means that we cannot reliably evaluate the R_* dependence predicted by the Andreas (1987) model, except perhaps at small R_* , where the data tend more toward the model than toward the artificial regression line. The artificial correlation, however, does not influence the mean value of z_T/z_0 . The model and the data in Fig. A1 tend to agree that, for R_* between 0.1 and 10, the typical value for z_T/z_0 is 1.

Although I have not made similar calculations for the other four datasets, because of (A.16), (A.17), and (A.20), $\ln(z_s/z_0)$ in all of these should decrease with increasing $\ln R_*$ if the data are strongly influenced by artificial correlation caused by the shared z_0 . Clearly, the data in Figs. 4, 6, and 7 display this trend. My reanalysis of Ishikawa and Kodama's (1994) data, shown in Fig. 5, shows a positive trend between z_T/z_0 and R_* , however. To produce this trend, z_T or z_0 in this dataset must be correlated with some of the other variables [see (A.14)], either physically or as a consequence of my analysis procedure. Thus, again, the data tend to corroborate the mean z_T/z_0 level predicted by the model but are ambiguous when it comes to testing the model's predicted R_* dependence.

From (A.16), we can infer some ways to minimize the fictitious correlation in plots of z_s/z_0 versus R_* . For example, if the standard deviation of $\ln z_0$, $s_{\ln z_0}$, is small compared to $s_{\ln z_s}$, the fictitious correlation—quantified by ρ in (A.16)—is small. Likewise, if the u_* range is large so that $s_{\ln u_*}$ is much larger than $s_{\ln z_0}$, (A.16) also predicts that ρ is small.

REFERENCES

- Andreas, E. L., 1987: A theory for the scalar roughness and the scalar transfer coefficients over snow and sea ice. *Bound.-Layer Meteor.*, **38**, 159–184.
- , 1995: Air–ice drag coefficients in the western Weddell Sea: 2. A model based on form drag and drifting snow. *J. Geophys. Res.*, **100**, 4833–4843.
- , 1998: The atmospheric boundary layer over polar marine surfaces. *Physics of Ice-Covered Seas*, Vol. 2, M. Leppäranta, Ed., Helsinki University Press, 715–773.
- , and K. J. Claffey, 1995: Air–ice drag coefficients in the western Weddell Sea: 1. Values deduced from profile measurements. *J. Geophys. Res.*, **100**, 4821–4831.
- Banke, E. G., S. D. Smith, and R. J. Anderson, 1980: Drag coefficients at AIDJEX from sonic anemometer measurements. *Sea Ice Processes and Models*, R. S. Pritchard, Ed., University of Washington Press, 430–442.
- Barry, P. J., and R. E. Munn, 1967: Use of radioactive tracers in studying mass transfer in the atmospheric boundary layer. *Phys. Fluids*, **10**, S263–S266.
- Beljaars, A. C. M., and A. A. M. Holtslag, 1991: Flux parameterization over land surfaces for atmospheric models. *J. Appl. Meteor.*, **30**, 327–341.
- Bintanja, R., and M. R. Van den Broeke, 1995: Momentum and scalar transfer coefficients over aerodynamically smooth Antarctic surfaces. *Bound.-Layer Meteor.*, **74**, 89–111.
- , and C. Reijmer, 2001: A simple parameterization for snowdrift sublimation over Antarctic snow surfaces. *J. Geophys. Res.*, **106**, 31 739–31 748.
- Brutsaert, W., 1975: A theory for local evaporation (or heat transfer) from rough and smooth surfaces at ground level. *Water Resour. Res.*, **11**, 543–550.
- , 1982: *Evaporation into the Atmosphere: Theory, History, and Applications*. D. Reidel, 299 pp.
- Busch, N. E., 1973: On the mechanics of atmospheric turbulence. *Workshop on Micrometeorology*, D. A. Haugen, Ed., Amer. Meteor. Soc., 1–65.
- Businger, J. A., 1973: Turbulent transfer in the atmospheric surface layer. *Workshop on Micrometeorology*, D. A. Haugen, Ed., Amer. Meteor. Soc., 67–100.
- , J. C. Wyngaard, Y. Izumi, and E. F. Bradley, 1971: Flux–profile relationships in the atmospheric surface layer. *J. Atmos. Sci.*, **28**, 181–189.
- Calanca, P., 2001: A note on the roughness length for temperature over melting snow and ice. *Quart. J. Roy. Meteor. Soc.*, **127**, 255–260.
- Canuto, V. M., A. Howard, Y. Cheng, and M. S. Dubovikov, 2001: Ocean turbulence. Part I: One-point closure model—Momentum and heat vertical diffusivities. *J. Phys. Oceanogr.*, **31**, 1413–1426.
- Carson, D. J., and P. J. R. Richards, 1978: Modelling surface turbulent fluxes in stable conditions. *Bound.-Layer Meteor.*, **14**, 67–81.
- Chamberlain, A. C., 1983: Roughness length of sea, sand, and snow. *Bound.-Layer Meteor.*, **25**, 405–409.
- Coantic, M., and B. Seguin, 1971: On the interaction of turbulent and radiative transfers in the surface layer. *Bound.-Layer Meteor.*, **1**, 245–263.
- Dyer, A. J., 1974: A review of flux–profile relationships. *Bound.-Layer Meteor.*, **7**, 363–372.
- Garratt, J. R., and B. B. Hicks, 1973: Momentum, heat and water vapour transfer to and from natural and artificial surfaces. *Quart. J. Roy. Meteor. Soc.*, **99**, 680–687.
- , and R. A. Brost, 1981: Radiative cooling effects within and above the nocturnal boundary layer. *J. Atmos. Sci.*, **38**, 2730–2746.
- Goodison, B., 1970: The relation between ablation and global radiation over Peyto Glacier, Alberta. *Glaciers, Proc. Workshop Seminar*, Ottawa, ON, Canada, Canadian National Committee for the International Hydrological Decade, 39–42.
- Heinemann, G., and L. Rose, 1990: Surface energy balance, parameterizations of boundary-layer heights and the application of resistance laws near an Antarctic ice shelf front. *Bound.-Layer Meteor.*, **51**, 123–158.
- Hicks, B. B., 1976: Wind profile relationships from the ‘Wangara’ experiment. *Quart. J. Roy. Meteor. Soc.*, **102**, 535–551.
- , 1978: Some limitations of dimensional analysis and power laws. *Bound.-Layer Meteor.*, **14**, 567–569.
- , and H. C. Martin, 1972: Atmospheric turbulent fluxes over snow. *Bound.-Layer Meteor.*, **2**, 496–502.
- Högström, U., 1988: Non-dimensional wind and temperature profiles in the atmospheric surface layer: A re-evaluation. *Bound.-Layer Meteor.*, **42**, 55–78.
- , 1996: Review of some basic characteristics of the atmospheric surface layer. *Bound.-Layer Meteor.*, **78**, 215–246.
- Holtslag, A. A. M., and H. A. R. de Bruin, 1988: Applied modeling of the nighttime surface energy balance over land. *J. Appl. Meteor.*, **27**, 689–704.
- Howell, J. F., and J. Sun, 1999: Surface-layer fluxes in stable conditions. *Bound.-Layer Meteor.*, **90**, 495–520.
- Inoue, J., 1989: Surface drag over the snow surface of the Antarctic Plateau: 1. Factors controlling surface drag over the katabatic wind region. *J. Geophys. Res.*, **94**, 2207–2217.
- Ishikawa, N., and Y. Kodama, 1994: Transfer coefficients of sensible heat on a snowmelt surface. *Meteor. Atmos. Phys.*, **53**, 233–240.

- Jackson, B. S., and J. J. Carroll, 1978: Aerodynamic roughness as a function of wind direction over asymmetric surface elements. *Bound.-Layer Meteor.*, **14**, 323–330.
- Joffre, S. M., 1982: Momentum and heat transfers in the surface layer over a frozen sea. *Bound.-Layer Meteor.*, **24**, 211–229.
- Jordan, R. E., E. L. Andreas, and A. P. Makshtas, 1999: Heat budget of snow-covered sea ice at North Pole 4. *J. Geophys. Res.*, **104**, 7785–7806.
- , —, and —, 2001: Modeling the surface energy budget and the temperature structure of snow and brine-snow at Ice Station Weddell. Preprints, *Sixth Conf. on Polar Meteorology and Oceanography*, San Diego, CA, Amer. Meteor. Soc., 129–132.
- Kader, B. A., and A. M. Yaglom, 1990: Mean fields and fluctuation moments in unstably stratified turbulent boundary layers. *J. Fluid Mech.*, **212**, 637–662.
- Kenney, B. C., 1982: Beware of spurious self-correlations! *Water Resour. Res.*, **18**, 1041–1048.
- Kim, J., and L. Mahrt, 1992: Simple formulation of turbulent mixing in the stable free atmosphere and nocturnal boundary layer. *Tellus*, **44**, 381–394.
- Kind, R. J., 1976: A critical examination of the requirements for model simulation of wind-induced erosion/deposition phenomena such as drifting snow. *Atmos. Environ.*, **10**, 219–227.
- King, J. C., and P. S. Anderson, 1994: Heat and water vapour fluxes and scalar roughness lengths over an Antarctic ice shelf. *Bound.-Layer Meteor.*, **69**, 101–121.
- , —, M. C. Smith, and S. D. Mobbs, 1996: The surface energy and mass balance at Halley, Antarctica during winter. *J. Geophys. Res.*, **101**, 19 119–19 128.
- Kondo, J., and H. Yamazawa, 1986: Bulk transfer coefficient over a snow surface. *Bound.-Layer Meteor.*, **34**, 123–135.
- , O. Kanechika, and N. Yasuda, 1978: Heat and momentum transfers under strong stability in the atmospheric surface layer. *J. Atmos. Sci.*, **35**, 1012–1021.
- Large, W. G., and S. Pond, 1981: Open ocean momentum flux measurements in moderate to strong winds. *J. Phys. Oceanogr.*, **11**, 324–336.
- , and —, 1982: Sensible and latent heat flux measurements over the ocean. *J. Phys. Oceanogr.*, **12**, 464–482.
- Launiainen, J., 1995: Derivation of the relationship between the Obukhov stability parameter and the bulk Richardson number for flux-profile studies. *Bound.-Layer Meteor.*, **76**, 165–179.
- , and T. Vihma, 1990: Derivation of turbulent surface fluxes—An iterative flux-profile method allowing arbitrary observing heights. *Environ. Software*, **5**, 113–124.
- , and B. Cheng, 1998: Modelling of ice thermodynamics in natural water bodies. *Cold Regions Sci. Technol.*, **27**, 153–178.
- Lettau, H. H., 1957: Summary of non-dimensional characteristics of boundary layer theory. *Exploring the Atmosphere's First Mile*, H. H. Lettau and B. Davidson, Eds., Pergamon Press, 337–372.
- , 1979: Wind and temperature profile prediction for diabatic surface layers including strong inversion cases. *Bound.-Layer Meteor.*, **17**, 443–464.
- Liu, W. T., K. B. Katsaros, and J. A. Businger, 1979: Bulk parameterization of air-sea exchanges of heat and water vapor including the molecular constraints at the interface. *J. Atmos. Sci.*, **36**, 1722–1735.
- Lyons, R., H. A. Panofsky, and S. Wollaston, 1964: The critical Richardson number and its implications for forecast problems. *J. Appl. Meteor.*, **3**, 136–142.
- Mahrt, L., 1981: Modelling the depth of the stable boundary-layer. *Bound.-Layer Meteor.*, **21**, 3–19.
- , 1998: Stratified atmospheric boundary layers and breakdown of models. *Theor. Comp. Fluid Dyn.*, **11**, 263–279.
- Monin, A. S., and A. M. Yaglom, 1971: *Statistical Fluid Mechanics: Mechanics of Turbulence*. Vol. 1. The MIT Press, 769 pp.
- Morris, E. M., 1989: Turbulent transfer over snow and ice. *J. Hydrol.*, **105**, 205–223.
- Munro, D. S., 1989: Surface roughness and bulk heat transfer on a glacier: Comparison with eddy correlation. *J. Glaciol.*, **35**, 343–348.
- Narasimha, R., and A. S. Vasudeva Murthy, 1995: The energy balance in the Ramdas layer. *Bound.-Layer Meteor.*, **76**, 307–321.
- Nieuwstadt, F. T. M., 1984: The turbulent structure of the stable nocturnal boundary layer. *J. Atmos. Sci.*, **41**, 2202–2216.
- Okamoto, M., and E. K. Webb, 1970: The temperature fluctuations in stable stratification. *Quart. J. Roy. Meteor. Soc.*, **96**, 591–600.
- Owen, P. R., 1964: Saltation of uniform grains in air. *J. Fluid Mech.*, **20**, 225–242.
- Panofsky, H. A., 1963: Determination of stress from wind and temperature measurements. *Quart. J. Roy. Meteor. Soc.*, **89**, 85–94.
- Paulson, C. A., 1970: The mathematical representation of wind speed and temperature profiles in the unstable atmospheric surface layer. *J. Appl. Meteor.*, **9**, 857–861.
- Plate, E. J., 1971: *Aerodynamic Characteristics of Atmospheric Boundary Layers*. U.S. Atomic Energy Commission, 190 pp.
- Raupach, M. R., 1992: Drag and drag partition on rough surfaces. *Bound.-Layer Meteor.*, **60**, 375–395.
- Sorbjan, Z., 1989: *Structure of the Atmospheric Boundary Layer*. Prentice Hall, 317 pp.
- Tennekes, H., and J. L. Lumley, 1972: *A First Course in Turbulence*. The MIT Press, 300 pp.
- Thom, A. S., 1971: Momentum absorption by vegetation. *Quart. J. Roy. Meteor. Soc.*, **97**, 414–428.
- Thorpe, M. R., E. G. Banke, and S. D. Smith, 1973: Eddy correlation measurements of evaporation and sensible heat flux over Arctic sea ice. *J. Geophys. Res.*, **78**, 3573–3584.
- Vihma, T., 1995: Subgrid parameterization of surface heat and momentum fluxes over polar oceans. *J. Geophys. Res.*, **100**, 22 625–22 646.
- Viswanadham, Y., 1979: Relation of Richardson number to the curvature of the wind profile. *Bound.-Layer Meteor.*, **17**, 537–544.
- , 1982: Examination of the empirical flux-profile models in the atmospheric surface layer. *Bound.-Layer Meteor.*, **22**, 61–77.
- Webb, E. K., 1970: Profile relationships: The log-linear range, and extension to strong stability. *Quart. J. Roy. Meteor. Soc.*, **96**, 67–90.
- Wieringa, J., 1980: A reevaluation of the Kansas mast influence on measurements of stress and cup anemometer overspeeding. *Bound.-Layer Meteor.*, **18**, 411–430.
- Woods, J. D., 1969: On Richardson's number as a criterion for laminar-turbulent-laminar transition in the ocean and atmosphere. *Radio Sci.*, **4**, 1289–1298.
- Yaglom, A. M., 1977: Comments on wind and temperature flux-profile relationships. *Bound.-Layer Meteor.*, **11**, 89–102.
- Yamamoto, G., 1975: Generalization of the KEYPS formula in diabatic conditions and related discussion on the critical Richardson number. *J. Meteor. Soc. Japan*, **53**, 189–195.